

## A high resolution infrared radiative transfer scheme to study the interaction of radiation with cloud

By W. T. ROACH and A. SLINGO  
*Meteorological Office, Bracknell*

(Received 3 August 1978; revised 18 January 1979)

### SUMMARY

This paper describes a high resolution radiative transfer scheme which calculates infrared fluxes and heating rates in a cloudy atmosphere. It is intended as a research tool for use in studies of the role of radiation in the physics of fog and layer cloud. The spectrum is split into five bands and allowance is made for molecular absorption by the water vapour  $6.3 \mu\text{m}$  band and the rotation band beyond  $20 \mu\text{m}$ , the  $15 \mu\text{m}$  carbon dioxide band, the  $9.6 \mu\text{m}$  ozone band, and the continuum absorption by water vapour in the  $10 \mu\text{m}$  atmospheric window. The strong absorption by cloud water droplets is calculated directly from the droplet size distribution function. The scheme has been run with a model stratocumulus cloud included, using data based on tethered balloon observations at Cardington. A large cooling rate of  $8.7 \text{ K per hour}$  is shown to exist at the cloud top.

### 1. INTRODUCTION

The interaction of clouds with the radiation field they produce is a complex and relatively neglected interdisciplinary subject which has only recently begun to attract detailed attention. The study of Arctic stratus cloud by Herman and Goody (1976) is a good example of this new interest. Roach (1976) has suggested on theoretical grounds that the growth of droplets in the top of layer cloud or fog is controlled by radiative loss, and numerical models incorporating this effect have produced realistic time scales for fog formation (Brown and Roach 1976).

The radiative transfer scheme described in this paper was developed initially as a diagnostic tool for use in studies of the role of radiation in fog and layer cloud. It is designed to cope with the large gradients in optical density (and consequently large cooling rates) found in cloud and fog tops and also with the need for increased spatial resolution near the level at which radiative fluxes and heating rates are computed. The scheme might have more general application in cloud-radiation interaction studies and modelling, provided the cloud can be assumed to be horizontally stratified on a scale large compared with the convective eddies within the cloud which might be induced by the radiation field. Liberal use is made of the many time-saving approximations developed in recent years, descriptions of which may be found in Goody (1964), Rodgers and Walshaw (1966) and Paltridge and Platt (1976).

The radiative fluxes and heating rates for a clear sky atmospheric profile are compared with the predictions of two other radiation schemes and the agreement is shown to be satisfactory. To demonstrate the large cooling rates which can exist at cloud tops, the scheme has also been run with data based on measurements of nocturnal stratocumulus obtained with the tethered balloon facility at Cardington (Roach *et al.*, to be published). A cooling rate of  $8.7 \text{ K per hour}$  is found for the layer  $1 \text{ mb}$  thick at the top of the cloud.

### 2. THEORY

In order to calculate the radiative heating rate, the equation of radiative transfer must be solved. In the infrared the effects of absorption by atmospheric gases and water droplets

dominate over those of scattering, which simplifies the problem considerably. The upward and downward fluxes,  $F_i(p) \uparrow$  and  $F_i(p) \downarrow$ , the net flux  $F_{i,net}(p) \uparrow$ , and the heating rate,  $H(p)$ , in spectral interval  $i$  at pressure  $p$ , are given by (e.g. Rodgers and Walshaw 1966):

$$F_i(p) \uparrow = \{B_i(g) - B_i(p_s)\} T_i(p, p_s) + B_i(p) - \int_{p_s}^p T_i(p, p') \{dB_i(p')/dp'\} dp' \quad (1)$$

$$F_i(p) \downarrow = \{B_i(\text{top}) - B_i(p_{\text{top}})\} T_i(p, p_{\text{top}}) + B_i(p) + \int_p^{p_{\text{top}}} T_i(p, p') \{dB_i(p')/dp'\} dp' \quad (2)$$

$$F_{i,net}(p) \uparrow = F_i(p) \uparrow - F_i(p) \downarrow \quad (3)$$

$$H(p) = (g/c_p) d\{\sum_i F_{i,net}(p) \uparrow\}/dp \quad (4)$$

where  $B_i(p)$  is the Planck function flux corresponding to the temperature of the air at the pressure  $p$ ,  $p_s$  the surface pressure, and  $p_{\text{top}}$  the lowest pressure to which the integration is taken. The net downward flux at this pressure is given by  $B_i(\text{top})$  and the contribution from the ground by  $B_i(g)$ .  $T_i(p, p')$  is the slab transmissivity between pressures  $p$  and  $p'$ . The acceleration due to gravity and specific heat at constant pressure vary little with pressure and atmospheric constitution and are assumed constant ( $g = 9.80665 \text{ m s}^{-2}$  and  $c_p = 1004 \text{ J kg}^{-1} \text{ K}^{-1}$ ).

The simple exponential attenuation law which applies for monochromatic radiation, known as Beer's law, is not obeyed over the wide spectral intervals occupied by the absorption bands of the principal gaseous absorbers (water vapour, carbon dioxide and ozone) because of the rapid variation of the absorption coefficient with frequency. The central problem in computing the heating rates therefore becomes that of using as small a number of spectral intervals as possible in order to avoid excessive computing time, whilst maintaining a reasonable accuracy in the calculation of the transmissivity averaged over these intervals.

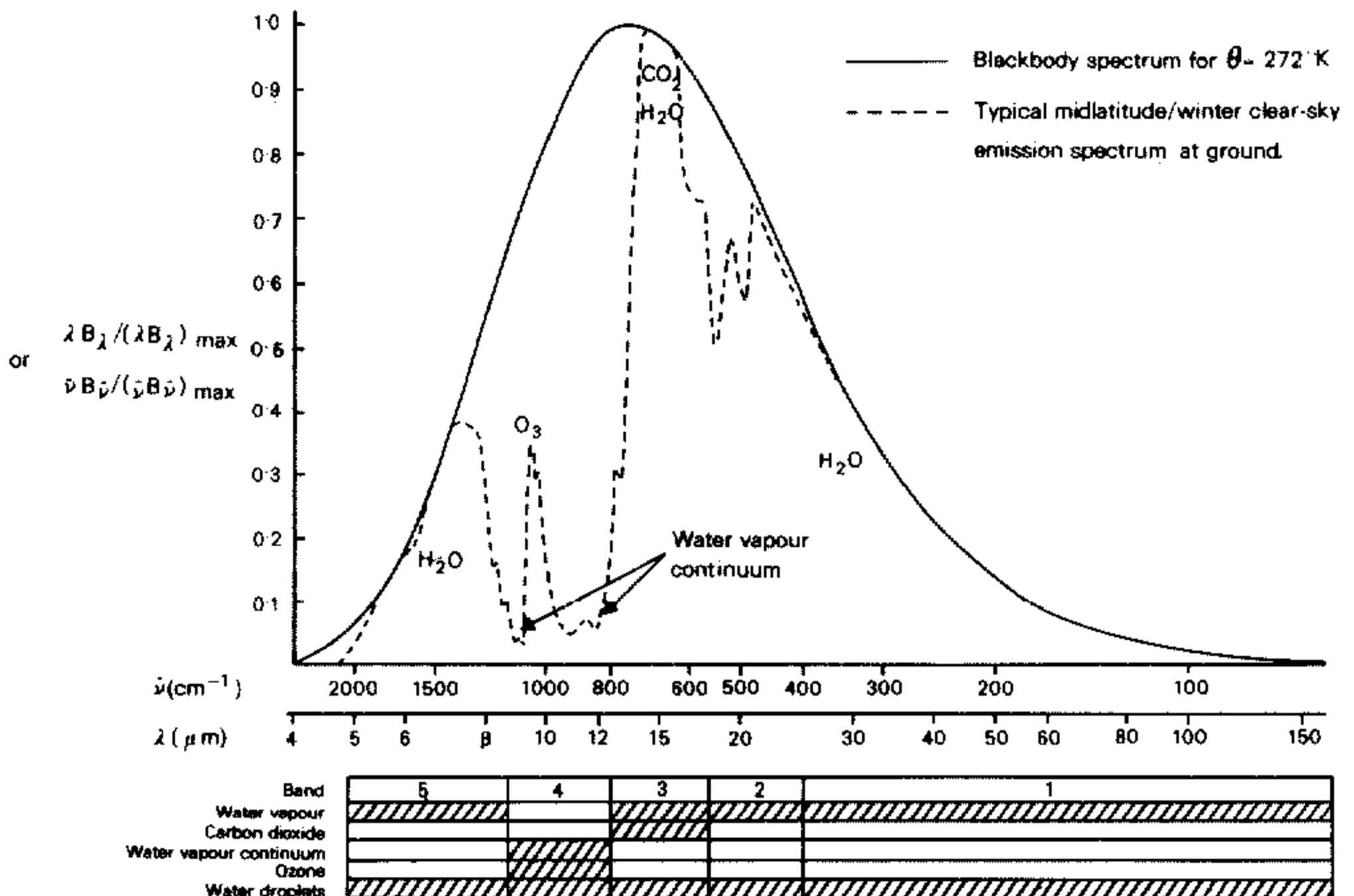


Figure 1. Principal absorbers and band limits of the radiation scheme.

The effect of the principal gaseous absorbers on a typical infrared emission spectrum is illustrated in Fig. 1. The opacity of the atmosphere is greatest where the emission spectrum meets the black-body spectrum, given by the Planck function for a temperature of 272 K. The principal spectral features are the strong absorption by water vapour in the  $6.3 \mu\text{m}$  vibration-rotation band and the rotation band beyond about  $20 \mu\text{m}$ , the strong absorption by carbon dioxide in the  $15 \mu\text{m}$  vibration-rotation band, and the region of low opacity at  $8\text{--}12 \mu\text{m}$ , known as the atmospheric window, in which there is only the weak absorption due to ozone at  $9.6 \mu\text{m}$  and the background water vapour continuum. The key at the bottom of Fig. 1 shows the limits of the five spectral bands used in the present scheme and the hatched areas show the absorbers which are taken into account in computing the transmissivities in each band. The important new feature is the calculation of the absorption by water droplets, which allows the scheme to be used in the study of the interaction of radiation with clouds and fog. Water droplets show strong continuous absorption throughout the infrared region of the spectrum, including the atmospheric window, so that clouds dominate the transfer of radiation within the troposphere.

(a) Calculation of  $B_i(p)$

The position of the maximum and the area beneath the Planck function curve, and hence the value of the flux in each spectral band, are strong functions of temperature. It was found that this temperature dependence could be taken into account by fitting the fluxes in each band by functions of the form

$$B_i(p) = a_i \theta^{b_i}(p), \quad i = 1, 5, \quad \dots \quad (5)$$

where  $B_i(p)$  is measured in  $\text{W m}^{-2}$  and  $\theta(p)$  is the temperature in K of the air at pressure  $p$ .

TABLE 1. VALUES OF  $a_i$  AND  $b_i$  IN EQ. (5)

Band $i$	Spectral range ( $\text{cm}^{-1}$ )	$a_i$	$b_i$
1	0-400	$8.961 \times 10^{-4}$	1.991
2	400-560	$4.676 \times 10^{-6}$	2.906
3	560-800	$2.637 \times 10^{-8}$	3.889
4	800-1150	$6.119 \times 10^{-12}$	5.360
5	1150-2050	$3.069 \times 10^{-18}$	7.844

The values of the coefficients  $a_i$  and  $b_i$  for each band are listed in Table 1. These were found by integrating the Planck function over each of the bands for the range of temperatures 200-300 K and obtaining a least-squares fit to Eq. (5).

3. CALCULATION OF THE TRANSMISSIVITY -  $T_i(p, p')$

The total transmissivity over any given path is found by multiplying together the transmissivities for each of the absorbers. In bands where an absorber is unimportant its transmissivity is set to unity. This multiplicative property of the transmissivities is a result of the essentially random overlapping of the individual absorption spectra within each band (Goody 1964, page 123). The methods used to calculate  $T_i(p, p')$  for the molecular bands, water vapour continuum, and water droplets are quite distinct and will be described in turn.

(a) *Molecular bands*

The method normally employed to calculate molecular transmissivities uses either laboratory or band model data to construct a single curve of transmissivity against absorber amount for a particular spectral interval, and to approximate this with an analytic function or look-up table. The required transmissivity is then found by scaling the absorber amount to take account of the integration over zenith angle and the dependence of the absorption on pressure and temperature. In the present scheme analytic fits to band model data are used. The random band model developed by Hunt and Mattingly (1976), which gives transmissivities in good agreement with laboratory data, was used with the molecular line compilation of McClatchey *et al.* (1973). Analytic functions were fitted at a temperature of 263 K and 1000 mb pressure. For the 15  $\mu\text{m}$  carbon dioxide band the function used was

$$T(u) = u_0^n / (u_0^n + u^n) \quad (6)$$

where  $u$  is the absorber amount measured in  $\text{g cm}^{-2}$  and  $u_0$  and  $n$  are constants.

Figure 2 illustrates the transmissivity as a function of absorber amount for this band. The fit to the data is extremely good over the range required (the minimum pathlength is  $5 \times 10^{-4} \text{g cm}^{-2}$  for 1 mb resolution, the maximum pathlength is  $5 \times 10^{-1} \text{g cm}^{-2}$  for 1000 mb surface pressure). Similar functions were used for water vapour, except that an extra term was required in bands 1 and 2 to fit the curves to a similar accuracy:

$$T(u) = u_0^n / (u_0^n + u^n + cu). \quad (7)$$

Also shown in Fig. 2 is Beer's law of exponential attenuation, which illustrates the fact that the wider the spectral band considered, the slower is the resultant change of transmissivity with absorber amount.

Equations (1) and (2) contain an implicit integration over zenith angle, whereas the transmissivity data refer to transmission of parallel radiation. It is possible to re-write the equations to perform this integration but it has been shown that an error of typically only 1–2 per cent in the heating rates is incurred by simply multiplying the absorber amounts by the 'diffusivity factor',  $D$ , which has the average value 1.66 (Goody 1964, page 243; Rodgers and Walshaw 1966).

The second important correction to the absorber amount takes account of the variations of the spectral line widths and intensities with temperature and pressure, so that the transmissivities are functions of these variables throughout the path between  $p$  and  $p'$ . It is usual to take account of this by means of the Curtis–Godson approximation (Goody 1964,

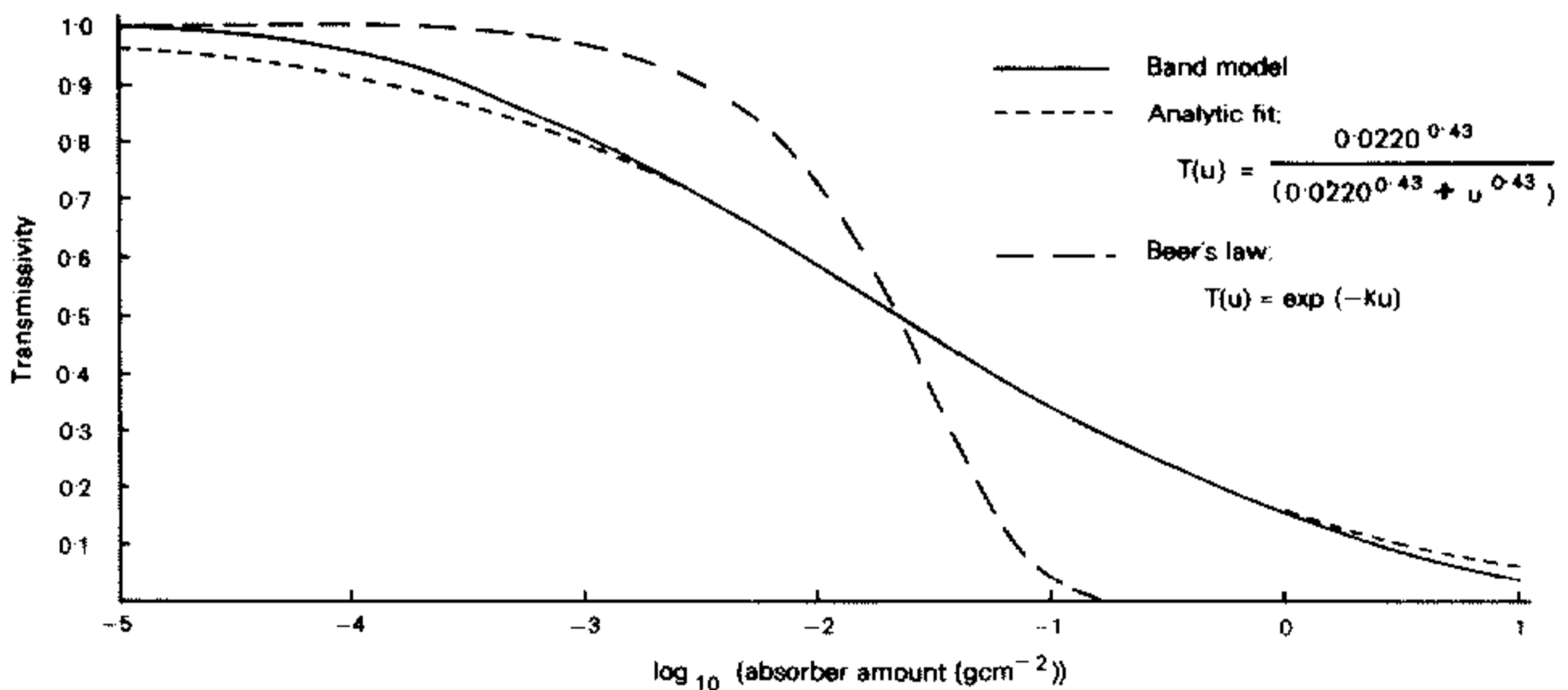


Figure 2. Transmissivity as a function of absorber amount for the 15  $\mu\text{m}$   $\text{CO}_2$  band ( $560\text{--}800 \text{cm}^{-1}$ ) at 263 K and 1000 mb. Beer's law of simple exponential attenuation is also shown.

page 237), by which an average absorber amount  $u^*$  and pressure  $p^*$  are derived. The functions used in the present scheme are:

$$[u^*]_p^{p'} = (1/g) \int_p^{p'} \phi(\theta)x(p'') dp'' \quad (8)$$

$$[u^*p^*]_p^{p'} = (1/g) \int_p^{p'} \phi(\theta)x(p'')p'' dp'' \quad (9)$$

where 
$$\phi(\theta) = (\theta_0/\theta)^q \quad (10)$$

The integrals are from  $p$  to  $p'$  and  $x(p'')$  is the mass mixing ratio of the gas. For water vapour this is the humidity mixing ratio and for carbon dioxide a constant mass mixing ratio of  $4.86 \times 10^{-4}$  is assumed.  $\theta_0$ , the reference temperature used in the band model calculations, is 263 K, and the value of  $q$  is derived from the lateral shift of the transmissivity curves with temperature, which is caused by the temperature dependence of the line shapes and also by the temperature dependence of the Planck function.

The effect of these two adjustments may be summarized:

$$T_i(p,p') = T(Du^*(p^*/p_0)^r) \quad (11)$$

where  $p_0$  is a reference pressure, taken to be 1000 mb. The values of the constants  $u_0$ ,  $n$ ,  $c$ ,  $q$  and  $r$  for carbon dioxide and water vapour in each band are listed in Table 2.

TABLE 2. TRANSMISSION FUNCTION CONSTANTS FOR WATER VAPOUR AND CARBON DIOXIDE

Band <i>i</i>	Gas	$u_0$ (g cm <sup>-2</sup> )	<i>n</i>	<i>c</i>	<i>q</i>	<i>r</i>
1	H <sub>2</sub> O	0.00257	0.6	1.92	0	0.8
2	H <sub>2</sub> O	0.1289	0.6	0.33	-4	0.8
3	H <sub>2</sub> O	3.471	0.6	—	-3	0.8
3	CO <sub>2</sub>	0.0220	0.43	—	0	0.85
4	—	—	—	—	—	—
5	H <sub>2</sub> O	0.0661	0.4	—	-4	0.7

The heating effect of the 9.6 μm ozone band in the troposphere, where the immediate applications of this scheme arise, is very small compared with that of the other two gases and it was found that an adequate representation could be obtained by setting  $B_i(\text{top})$  equal to 3 W m<sup>-2</sup> in band 4,  $B_i(\text{top})$  being zero in the other bands. Should the need arise, ozone can easily be incorporated more accurately in the way described above for water vapour and carbon dioxide.

(b) *Water vapour continuum*

The atmospheric window from 8 to 12 μm contains, in addition to the ozone molecular band at 9.6 μm, the broad continuum absorption by water vapour. The absorption coefficient has a water vapour pressure-dependent component which is probably caused by the dimer molecule (H<sub>2</sub>O)<sub>2</sub> (Bignell 1970; Paltridge and Platt 1976, p. 161), whose effect on radiative transfer in the window can be very important. The continuum nature of the absorption spectrum means that the transmissivity due to water vapour in this region follows the simple exponential law:

$$T(p,p') = \exp(-\int k du) \quad (12)$$

where the integral is from  $u(p)$  to  $u(p')$ , and  $u$  is the absorber amount, scaled by the diffusi-

vity factor  $D$ . The mass absorption coefficient  $k$  can be separated into two terms due to the combined effect of the wings of distant strong lines and the dimer molecule:

$$k = k_1 p'' + k_2 e(p'') \quad (13)$$

where  $k_1 = 0.1 \text{ g}^{-1} \text{ cm}^2 \text{ atm}^{-1}$  and  $k_2 = 20 \text{ g}^{-1} \text{ cm}^2 \text{ atm}^{-1}$  at 263 K, and  $e$  is the water vapour pressure. Both coefficients are temperature dependent, the dependence being very strong in the case of the dimer, for which the absorption decreases rapidly with increasing temperature according to  $\exp(1745/\theta)$  (Lee 1973). An equivalent function is  $(263/\theta)^{6.5}$ , which is used here. Equation (12) can then be written

$$T(p, p') = \exp \left[ -\frac{D}{g} \int_p^{p'} \left\{ k_1 \phi_1(\theta) + \frac{k_2 \phi_2(\theta) x(p'')}{0.622} \right\} x(p'') p'' dp'' \right] \quad (14)$$

where  $\phi_1 = (263/\theta)^{-1.5}$  and  $\phi_2 = (263/\theta)^{6.5}$ .

### (c) Water droplets

Water droplets of the sizes commonly found in clouds and fogs (1–20  $\mu\text{m}$ ) absorb strongly throughout the infrared. The absorption spectrum of a single droplet can be computed from Mie theory (Van de Hulst 1957). The effect of the finite absorptivity of the water droplets and the fact that they are present with a range of sizes is to produce a continuous spectrum. Beer's law is therefore obeyed so the transmissivity due to the droplets can be written

$$T_i(p, p') = \exp \{ -\tau(p, p') \} \quad (15)$$

where the optical depth  $\tau(p, p')$  is the integral of the absorption cross-section  $\sigma_i(p'')$  over the path from  $p$  to  $p'$ . The absorption cross-section of all the water droplets at pressure  $p''$  for the  $i$ th spectral band is given by

$$\sigma_i(p'') = \int_0^\infty n(r, p'') Q_i(r) \pi r^2 dr \quad (16)$$

$n(r, p'')$  is the size distribution function of the droplets at pressure  $p''$ . Equation (16) is integrated numerically over 15 radius bins, allowing cloud droplet spectra obtained with a laser spectrometer probe (Knollenberg 1976) to be incorporated into the program as data.  $Q_i(r)$  is the absorption efficiency factor  $Q_a(r, \tilde{\nu})$  weighted over the wide spectral band by the Planck function:

$$Q_i(r) = \int Q_a(r, \tilde{\nu}) B(\tilde{\nu}, \theta_0) d\tilde{\nu} / \int B(\tilde{\nu}, \theta_0) d\tilde{\nu} \quad (17)$$

where the limits of the integrations are the edges of the  $i$ th band. In practice,  $Q_i(r)$  can be closely represented by an expression of the form (Herman 1962; Roach 1976)

$$Q_i(r) = \alpha_i \{ 1 - \exp(-\beta_i r) \} \quad (18)$$

TABLE 3. CONSTANTS USED TO CALCULATE  $Q_i(r)$

Band		
$i$	$\alpha_i$	$\beta_i$
1	See text	
2	1.6	0.25
3	1.35	0.45
4	1.13	0.16
5	1.3	0.1

The values of the constants  $\alpha_i$  and  $\beta_i$  are given in Table 3. They were derived using the data of Irvine and Pollack (1968). The rapid decrease of  $Q_a(r, \vec{v})$  with radius in band 1 results in a virtually linear function in this region, for which  $Q_i(r) = 1.3r$ , where  $r$  is measured in microns and  $Q_i(r)$  is limited to a maximum of 1.4.

Finally, Eq. (15) can be re-written

$$T_i(p, p') = \exp\left\{-\frac{\gamma_i N_A k}{Mg} \int_p^{p'} \frac{\sigma_i(p'') \theta}{p''} dp''\right\} \quad (19)$$

where  $N_A$  is Avogadro's constant,  $k$  is Boltzmann's constant and  $M$  is the mean molecular weight of air.  $\gamma_i$  is the droplet diffusivity factor whose value will now be derived.

#### (d) Scattering effects

Roughly half the infrared radiation intercepted by water droplets is scattered, predominantly in the forward direction, and some allowance for this must be made. However, in most of the spectrum the effect is small because the absorption by atmospheric gases is so large, but this situation is reversed in the window region. Multiple scattering increases the effective absorber amount because radiation which would otherwise leave the scattering volume can be scattered back into it and hence suffer additional absorption. Scattering of infrared radiation by water droplets can therefore be taken into account by increasing the droplet diffusivity factor. The diffusivity factor for droplets,  $\gamma_i$ , can be written (Herman and Goody 1976):

$$\gamma_i^2 = 3(1 - \tilde{\omega}_i \langle \cos\theta \rangle_i) / (1 - \tilde{\omega}_i) \quad (20)$$

where  $\langle \cos\theta \rangle_i$  is the scattering asymmetry factor and  $\tilde{\omega}_i$  is the single-scattering albedo averaged over the  $i$ th spectral band and over all the droplets:

$$\tilde{\omega}_i = \int_0^\infty n(r) \pi r^2 Q_{s_i}(r) dr / \int_0^\infty n(r) \pi r^2 Q_{e_i}(r) dr \quad (21)$$

$Q_{s_i}(r)$  and  $Q_{e_i}(r)$  are the scattering and extinction efficiency factors, respectively. It was found that the value of  $\gamma_i$  in the window region varies between 1.85 and 1.95 for a variety of size distribution functions  $n(r)$  so the droplet diffusivity factor has been increased to the value 1.9 in band 4 and kept at 1.73 in the other bands.

#### 4. INTEGRATION SCHEME

Vertical profiles of temperature, humidity and water droplet size distributions, expressed as number densities in 15 specified radius ranges, are interpolated on to a regularly spaced pressure grid, in preliminary programs. These data are accessed by the radiation scheme which calculates  $B_i(p)$  for each band and each pressure level using Eq. (5). The integrands of Eqs. (8), (9), (14) and (19) are calculated for each layer between these levels and the main integration loop entered to solve Eqs. (1)–(4).

The computer program used is normally run with 1000 levels, giving a maximum resolution of about 1 mb, corresponding to about 10 m at ground level. To solve Eqs. (1)–(4) with  $dp'$  set to 1 mb everywhere would be wasteful of computer time, however, as the integrals have to be recalculated for each level. To reduce computing time and take advantage of the fact that much of the absorption takes place close to the level of interest, the grid used is centred on this level and the grid size expands away in increasing steps, doubling  $dp'$  every five levels. The number of steps in the integration is thus reduced to about 40, whilst taking proper account of the absorber amounts in each step. Serious errors could

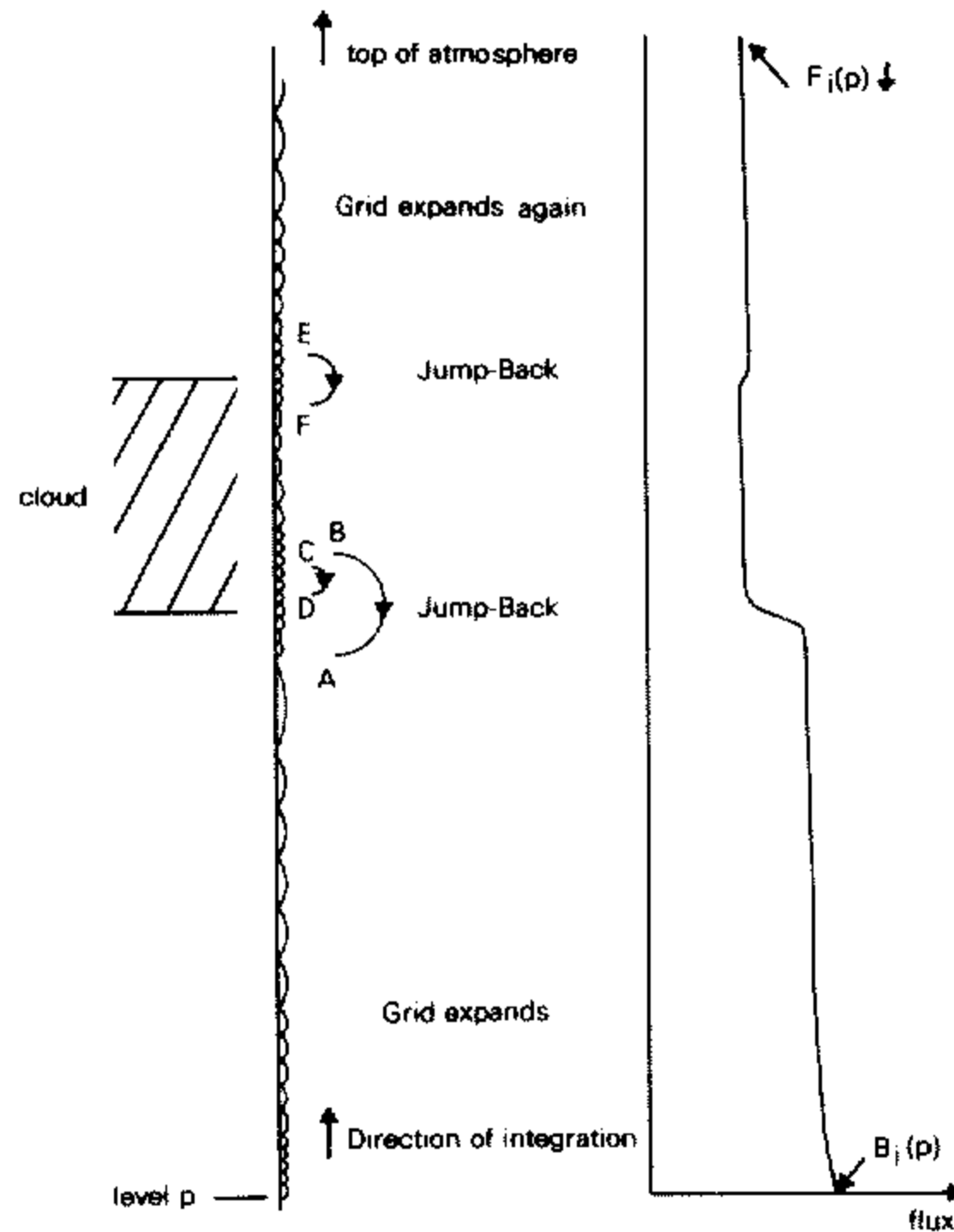


Figure 3. Illustrating the expanding grid and 'jump-back' facility. To calculate  $F_i(p) \downarrow$ , the integration commences at  $p$  and works up through the atmosphere doubling  $dp'$  every 5 levels. At B the integration enters the cloud with too coarse a resolution, jumps back to A and begins again with maximum resolution, as it also does from C to D and from E to F. After leaving the top of the cloud the grid expands unchecked to the top of the atmosphere. The graph on the right illustrates how the correct value of  $F_i(p) \downarrow$  is obtained. result if the integration traverses an inversion, or the edge of a cloud, with too coarse a resolution. In such situations the integrands in Eqs. (1) and (2) can be large and of either sign. The resolution of the scheme must therefore be a maximum at such levels, and this is achieved by continuously monitoring the rate of change of  $F_i(p) \uparrow$  and  $F_i(p) \downarrow$ . If a large change occurs the integration stops, jumps back to the last step, and proceeds with maximum resolution to encounter the feature, and then begins to expand the grid again. This 'jump-back' facility can operate at any level in the integration and its ability to deal with such features is illustrated in Fig. 3.

##### 5. COMPARISON WITH OTHER SCHEMES AND APPLICATIONS

Stone and Manabe (1968) compared the infrared radiation scheme of Rodgers and Walshaw (1966) with that of Manabe and Strickler (1964) and found that the two schemes gave very similar results for the fluxes and heating rates in a clear atmosphere. The present program has also been run with their data and the results are shown in Fig. 4. The three schemes are in broad agreement, predicting a uniform cooling of about 1.5–2.0 K per day, mainly due to water vapour, with a maximum just below the tropopause and a second maximum close to the ground, which is made more prominent in the present scheme by the inclusion of the water vapour continuum. The important role of the water vapour continuum in determining heating rates in the lower troposphere has been noted by many authors (see Paltridge and Platt 1976, pp. 161–164) and is the dominant cause of cooling at such levels in moist tropical atmospheres (Grassl 1974; Hunt and Mattingly 1976). The only major disagreement is in the treatment of carbon dioxide, for which the present scheme predicts a significantly smaller tropospheric cooling rate. The difference is probably due to the different methods of solving Eqs. (1)–(4), since the molecular data used are very similar

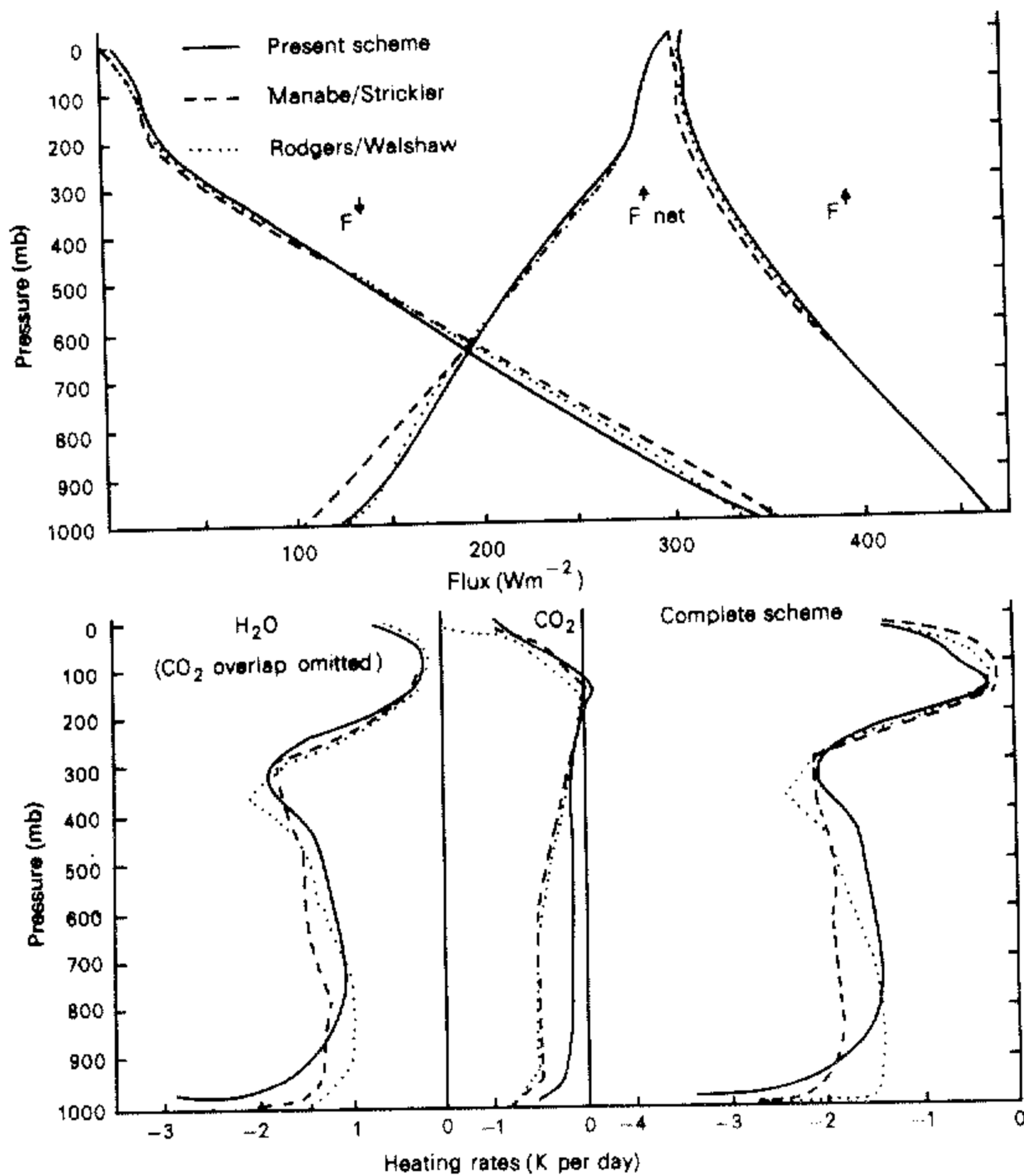


Figure 4. Comparison of the fluxes and heating rates of the present scheme with those of Manabe and Strickler (1964) and Rodgers and Walshaw (1966), using the data of Stone and Manabe (1968), with no clouds present.

to those of Stone and Manabe. It must be pointed out, however, that the present results agree well with those of Hunt and Mattingly (their Fig. 11), who used several different methods of treating carbon dioxide absorption, with consistent results for the troposphere.

In order to illustrate how clouds affect the transfer of radiation in the troposphere, the program has been run with a model stratocumulus cloud included. Figure 5 illustrates the data used, which are based on recent observations at Cardington. The cloud occupies the region between 910 and 950 mb, with a roughly linear increase of liquid water content with height. The mode droplet radius rises from about  $1\ \mu\text{m}$  at 950 mb to about  $9\ \mu\text{m}$  at 910 mb. The surface pressure was 1030 mb and surface temperature 281 K. 1000 levels were used giving a resolution of 1.03 mb, so that the cloud top is defined to this accuracy with a temperature change across the capping inversion of 5 K.

The results are illustrated in Fig. 6. Above the cloud the downward flux,  $F\downarrow$ , takes its clear sky value as it depends only on the atmospheric profile above the level at which it is calculated. Similarly, below the cloud the upward flux,  $F\uparrow$ , takes its clear sky value as it depends only on the profile below the cloud and on the ground temperature (281 K, corresponding to  $348\ \text{W m}^{-2}$ ). Within the cloud the water droplet absorption is very strong, so that the cloud is optically thick, and both upward and downward fluxes are therefore close to the Planck function flux corresponding to the temperature near the top of the cloud ( $306\ \text{W m}^{-2}$  at 271 K). The net upward flux falls rapidly to near zero on entering the top of

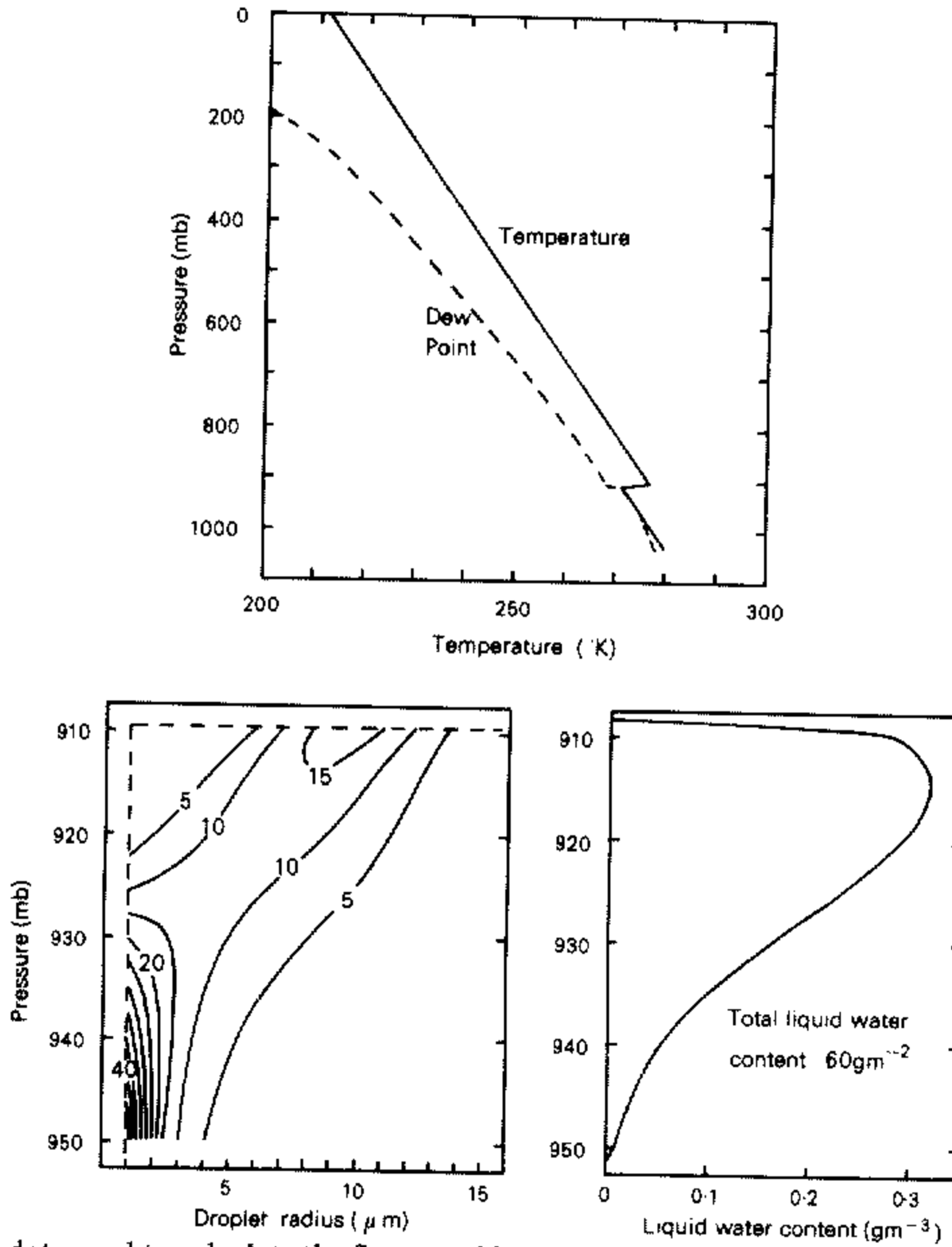


Figure 5. Cloud data used to calculate the fluxes and heating rates shown in Fig. 6. The contour plot shows isopleths of percentage normalized spectral density in 1 μm radius steps, such that at any given pressure the sum of the 15 values is 100.

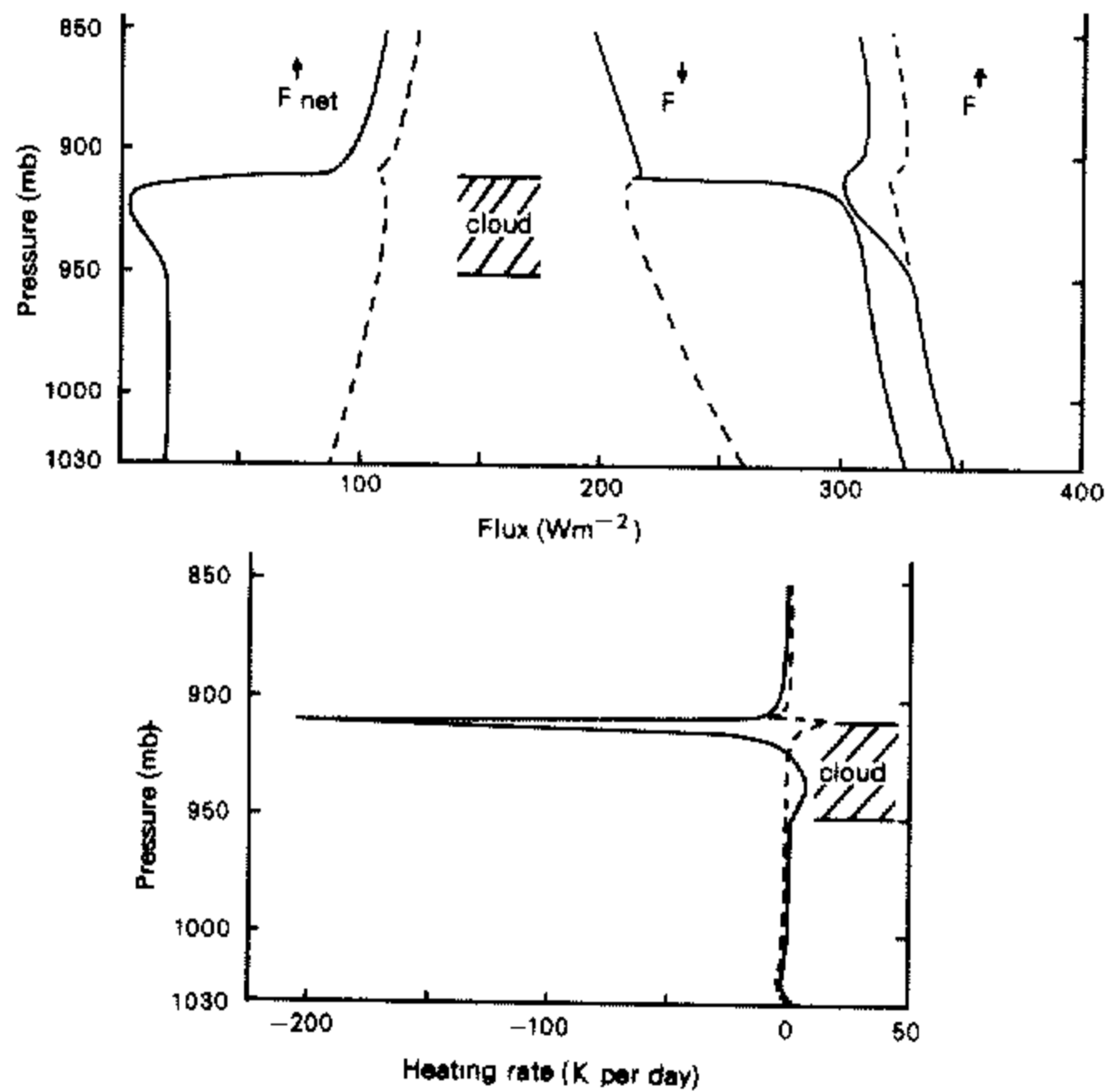


Figure 6. Illustrating the dominating effect of clouds on radiative transfer. The dashed lines indicate clear sky values of fluxes and heating rates and the solid lines indicate values when cloud is present.

the cloud because the optical depth here is large. It rises slowly towards the cloud base, where the optical depth is much smaller due to the lower droplet concentrations, reaching a nearly constant value below the cloud. The cloud top is therefore subject to strong radiational cooling which acts to maintain the capping temperature inversion. The cloud base is warmed by the net upward flux of radiation from the warmer atmosphere and ground beneath.

The sensitivity of the results to the value of the droplet diffusivity factor was investigated by setting it equal to 1.66 in all five spectral bands. The cooling was distributed more evenly through the cloud, the value at the cloud top being reduced by 9%. This is to be expected because reducing the droplet diffusivity factor also reduces the total optical thickness of the cloud.

Over distances of less than a few metres the atmosphere is transparent even in the strongest absorption bands, so that within this distance of the ground the air is no longer shielded from the direct influence of the ground term in Eq. (1). The heating rate close to the ground is therefore very sensitive to the contrast between air and ground temperatures. The latter is slightly higher in this case and accounts for the positive heating rates at the lowest levels.

From these results it is obvious that radiation plays a major role in the structure and evolution of layer cloud. The radiation scheme described in this paper is already being used to aid the interpretation of the data obtained on such cloud, using the tethered balloon facility at Cardington.

## REFERENCES

- |  |      |  |
|--|------|--|
| Bignell, K. J.   | 1970 | The water vapour infrared continuum, <i>Quart. J. R. Met. Soc.</i> , <b>96</b> , 390-403.  |
| Brown, R. and Roach, W. T.   | 1976 | The physics of radiation fog: II - a numerical study, <i>Ibid.</i> , <b>102</b> , 335-354.   |
| Goody, R. M.   | 1964 | <i>Atmospheric radiation</i> , Clarendon Press, Oxford.  |
| Grassl, H.   | 1974 | Influence of different absorbers in the window region on radiative cooling (and on surface temperature determination), <i>Contrib. Atmos. Phys.</i> , <b>47</b> , 1-13.  |
| Herman, B. M.  | 1962 | Infrared absorption, scattering and total attenuation cross-sections for water spheres, <i>Quart. J. R. Met. Soc.</i> , <b>88</b> , 143-150.   |
| Herman, G. F. and Goody, R.  | 1976 | Formation and persistence of summertime Arctic stratus clouds, <i>J. Atmos. Sci.</i> , <b>33</b> , 1537-1553.  |
| Hunt, G. E. and Mattingly, S. R.   | 1976 | Infrared radiative transfer in planetary atmospheres - I. Effects of computational and spectroscopic economies on thermal heating/cooling rates, <i>J. Quant. Spectrosc. Radiat. Transfer</i> , <b>16</b> , 505-520. |
| Irvine, W. M. and Pollack, J. B.   | 1968 | Infra-red optical properties of water and ice spheres, <i>Icarus</i> , <b>8</b> , 324-360.   |
| Knollenberg, R. G.   | 1976 | Three new instruments for cloud physics measurements, Preprint Vol., <i>Int. Conf. Cloud Physics</i> , Boulder, Colorado, 554-561.   |
| Lee, A. C. L.  | 1973 | A study of the continuum absorption within the 8-13 $\mu\text{m}$ atmospheric window, <i>Quart. J. R. Met. Soc.</i> , <b>99</b> , 490-505.   |
| Manabe, S. and Strickler, R. F.  | 1964 | Thermal equilibrium of the atmosphere with a convective adjustment, <i>J. Atmos. Sci.</i> , <b>21</b> , 361-385.   |
| McClatchey, R. A., Benedict, W. S.,<br>Clough, S. A., Burch, D. E.,<br>Calfee, R. F., Fox, K.,<br>Rothman, I. S. and Garing, J. S. | 1973 | AFCRL Atmospheric absorption line parameters compilation, <i>Environmental research paper</i> No. 434.   |
| Paltridge, G. W. and<br>Platt, C. M. R.  | 1976 | Radiative processes in meteorology and climatology, <i>Developments in atmospheric science</i> , <b>5</b> , Elsevier.  |
| Roach, W. T.   | 1976 | On the effect of radiative exchange on the growth by condensation of a cloud or fog droplet, <i>Quart. J. R. Met. Soc.</i> , <b>102</b> , 361-372.   |

- Rodgers, C. D. and  
Walshaw, C. D. 1966 The computation of infra-red cooling rate in planetary  
atmospheres, *Ibid.*, **92**, 67-92.
- Stone, H. M. and Manabe, S. 1968 Comparison among various numerical models designed for  
computing infra-red cooling, *Mon. Weath. Rev.*, **96**,  
735-741.
- Van de Hulst, H. C. 1957 *Light scattering by small particles*, John Wiley and Sons.